JOURNAL OF AIRCRAFT
Vol. 44, No. 3, May–June 2007

Extension of Projectile Range Using Oblique-Wing Concept

Lei Tang,* Danny D. Liu,† and P. C. Chen‡
ZONA Technology, Inc., Scottsdale, Arizona 85258

DOI: 10.2514/1.21194

An innovative projectile design is proposed using body-conformal oblique wing/tails with smart-structure control. With optimal deployments of the oblique wing, this guided projectile would maintain the maximum lift-to-drag ratio throughout its gliding phase, from supersonic through transonic to subsonic, and achieve an extended range which exceeds the maximum range required for the baseline rocket-assisted projectile. To search for the optimal sweepback positions of the oblique wing during the supersonic and transonic gliding phases, intensive thin-layer Reynolds-averaged Navier–Stokes computations are performed using the overset-grid approach. Based on the optimal scheduling of the oblique wing obtained from the Reynolds-averaged Navier–Stokes computations, our preliminary two degrees-of-freedom trajectory analysis indicates that the target 100 n mile range is achievable without rocket assistance.

I. Introduction

EXTENDED range guided munition (ERGM) projectile design for naval surface fire support (NSFS) aims at achieving the required range through a combination of rocket assistance and gliding flight. The rocket motor, however, has a negative impact on payload, cost, safety, reliability, etc., and so the current design strategy of NSFS is to eliminate the rocket motor from the ERGM projectile without sacrifice of its range requirement.

This challenging design strategy prompted ZONA Technology to come out with an innovative projectile design which uses body-conformal oblique wing/tails with smart-structure (actuator) control. As will be shown in this paper, with optimal deployments of the oblique wing during the supersonic and transonic gliding phases, this guided projectile would maintain the maximum lift-to-drag ratio (L/D) throughout its gliding phase and achieve an extended range which exceeds the maximum range required for the rocket-assisted ERGM.

The concept of using an oblique wing is not new. Its first use was proposed by the Germans during World War II. R. T. Jones further developed the theory and proposed its application for supersonic drag reduction and for sonic boom alleviation [1]. The Chance Vought BGM-110 also adopted an untapered oblique wing for its supersonic flight. But that was a rather primitive design in that the wing cut through the center body and the missile had no control capability [2].

The oblique wing has superior aerodynamic characteristics because it can maintain a subsonic leading edge throughout the supersonic/transonic ranges and significantly reduce the wave drag. In fact, it can achieve a much higher lift-to-drag ratio at all Mach numbers than virtually any other wing. If the wing is deployed near the apogee at a supersonic speed, maintaining the maximum lift-to-drag ratio of the projectile throughout the whole gliding phase requires the oblique wing to move to the optimal sweepback position at each trajectory point in a continuous manner with a simple, lightweight mechanism.

To search for the optimal sweepback positions of the oblique wing during the supersonic and transonic gliding phases, in the present work, intensive thin-layer Reynolds-averaged Navier–Stokes (RANS) computations are performed for a series of Mach numbers and angles of attack. The so-called overset-grid approach is adopted to avoid the tedious grid regeneration process for different deployments of the oblique wing. In this approach, after generating all component grids once, one only needs to rotate the wing and wing-cap grids to the new sweepback positions. Using the optimal scheduling of the oblique wing obtained from the RANS computations, our preliminary two degrees-of-freedom trajectory analysis further indicates that it is feasible for ERGM to achieve the target 100 n mile range without rocket assistance.

II. Numerical Methodology

The computational aerodynamic tool used in this study is CFL3D v6 [3],[§] which is developed and supported by NASA Langley Research Center. This is a three-dimensional thin-layer Reynolds-averaged Navier–Stokes code, using an implicit, approximately factored, finite volume, upwind, and multigrid algorithm. It employs formally third-order accurate upwind-biased spatial differencing for the inviscid terms with flux limiting in the presence of shocks. Either flux-difference or flux-vector splitting is available. The flux-difference splitting method of Roe [4] is employed in the present computations to obtain the numerical fluxes at cell faces. On the other hand, the viscous terms are discretized with the second-order central scheme. Numerous turbulence models are available in the code, whereas the Spalart–Allmaras one-equation model [5] is chosen in the present computations. A detailed description of the code is referred to in [3].

One of the important features of the CFL3D code is its capability of supporting overset grids. This is a very useful feature for the present computations because we intend to investigate the aerodynamic performances of the projectile with the wing at multiple sweep positions. Using the overset-grid approach can significantly save our grid generation efforts. In this approach, after generating all component grids once, we only need to rotate the wing and wing-cap grids to different wing positions.

Figure 1 presents the overset-grid systems around the projectile with the wing at three selected sweep positions. There are eight component grids total, which are generated with a hyperbolic grid generator, HYPGEN [6]. The grid around the body has 235 grid points along the longitudinal direction with clustering at the nose and near the wing and fins, 91 grid points along the azimuthal direction with clustering around the wing region, and 81 grid points in the normal direction with clustering near the surface. The first grid spacing from the surface is about $7 \times 10^{-6}c$ (for all component

Presented as Paper 4600 at the 23rd AIAA Applied Aerodynamics Conference, Toronto, Canada, 6–9 June 2005; received 16 November 2005; revision received 20 January 2006; accepted for publication 7 February 2006.

*Currently at D&P LLC, Phoenix, AZ 85018. AIAA Associate Fellow.
†President. AIAA Fellow.
‡Vice President. Senior Member AIAA.

§The user manual of CFL3D can be found at http://cfl3d.larc.nasa.gov/Cfl3dv6/cfl3dv6.html.

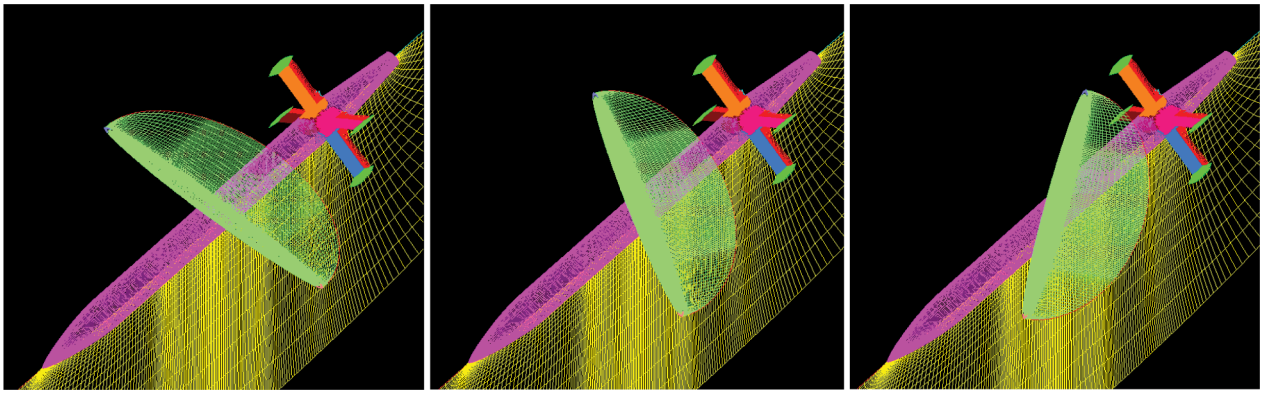

a) χ=90 deg (fully deployed) b) χ=60 deg c) χ=30 deg

Fig. 1 Overset-grid systems around the projectile.

grids), where c is the wing chord at the midspan. The outer boundary is extended to about $25c$. This grid also acts as a background grid to cover the whole computational domain. The grid around the wing has 161 grid points along the chord direction with 100 grid points on the body, 181 grid points in the spanwise direction with clustering near the body region, and 51 grid points in the normal direction with clustering near the surface. The outer boundary is extended to about $2c$. There are also two wing-cap grids. Each has $37 \times 49 \times 51$ grid points. The remaining four grids are generated for the four fins. Each has 133 grid points along the chord direction, 71 grid points in the spanwise direction with 41 points on the fin surface, and 51 points in the normal direction with clustering near the surface. The outer boundaries are also extended to about $2c$.

The establishment of communication between the preceding overset component grids is a very tedious job. One needs to find out which boundary points in a grid must be updated by the interpolated flow variables from the other grids and calculate the required interpolation coefficients for the grid points that send information to an interpolated boundary point in another grid. The standard overset-grid preprocessor for the CFL3D code is the MultiGeometry Grid Embedding (MaGGiE) code [7], which was initially developed from a very early version of PEGASUS at Old Dominion University and further modified by NASA Langley Research Center to increase its generality. Recently, a much more automated PEGASUS code [8] has been developed. To take advantage of this much more automated PEGASUS code, some efforts have been spent to allow use of PEGASUS-generated overset data files in CFL3D.

CFL3D adopts the cell-centered finite volume approach, whereas PEGASUS is written for the finite difference approach. And so, a new grid needs to be created first to fit PEGASUS. This new grid consists of the cell centers of the original grid plus the cell-face centers on all boundaries. The addition of the cell-face centers ensures that the new grid occupies the same physical domain as the original grid. The second step is to set up a PEGASUS input file based on the CFL3D input file and run PEGASUS. Note that XINTOUT, the output of PEGASUS, is created for the augmented cell-center grid. Therefore, the last step is to convert XINTOUT back to a format which fits CFL3D.[§]

The method used for a rough estimation of projectile range is a simple two degrees-of-freedom trajectory analysis. With $\gamma = \arctan(dy/dx)$, the equations of motion of the projectile can be written as

$$\begin{cases} m\ddot{x} = -L\sin\gamma - D\cos\gamma \\ m\ddot{y} = L\cos\gamma - D\sin\gamma - mg \end{cases} \tag{1}$$

where (x, y) is the position of the projectile center of mass, $(\ddot{x}, \ddot{y})$ is the corresponding acceleration, and m is the projectile mass. The aerodynamic lift force L and drag force D in (1) are computed by the preceding thin-layer RANS approach. The integration of Eq. (1) uses the simplest Euler scheme.

III. Results and Discussion

In this section, the results from the intensive thin-layer Reynolds-averaged Navier–Stokes computations are presented for five sweepback positions of the oblique wing ranging from 30 to 90 deg, 12 Mach numbers ranging from 0.2 to 1.4, and eight angles of attack ranging from 0 to 10 deg. From those computational results, the optimal sweep angle and angle of attack of the oblique wing at each Mach number are determined. Based on this optimal scheduling of the oblique wing, a simple two degrees-of-freedom trajectory analysis is further performed to determine the projectile range.

A. Aerodynamic Performances of the Projectile with Fully Deployed Wing at $\alpha = 0$ deg

Figure 2 presents the aerodynamic performances of the projectile with fully deployed wing at $\alpha = 0$ deg for M_∞ from 0.2 to 0.8. The selected reference area is the maximum body cross section area. It is found that the lift coefficient of the projectile increases slightly with increment of M_∞ from 0.2 to 0.7, whereas the drag coefficient decreases slightly. Therefore, the lift-to-drag ratio increases with the Mach number up to 0.7.

With increment of M_∞ from 0.7 to 0.8, however, the lift coefficient of the projectile decreases, whereas the drag coefficient increases, clearly indicating the transonic effects (mainly at the wing). Therefore, the lift-to-drag ratio of the projectile drops significantly. The aerodynamic performances of this projectile are found to be very similar to those of an airfoil.

Figure 3 further presents the pressure contours around the wing at the midspan for $M_\infty = 0.6$, 0.7, and 0.8. As expected, the whole flowfield is subsonic at $M_\infty = 0.6$, whereas a weak shock starts to form at $M_\infty = 0.7$. At $M_\infty = 0.8$, however, a strong shock already exists and causes the preceding drag divergence, and the drop of lift and lift-to-drag ratio. To achieve a higher lift-to-drag ratio for the cases of M_∞ greater than 0.7, therefore, we need to sweep the wing for reduction of the transonic effects.

B. Effect of Sweep Angles at $M_\infty = 0.8$

Figure 4 presents the variation of aerodynamic forces of the projectile with the sweep angle at $M_\infty = 0.8$. Note that our definition of the sweep angle χ here is different from the widely used definition of the sweep angle Λ. The relationship between these two sweep angles is $\chi = 90\,\text{deg} - \Lambda$. It is found that the lift coefficient of the projectile initially increases slightly with the sweep due to the weaker transonic effects and then drops with the sweep because the loss of lifting area starts to dominate the sweep effect. At the same time, the drag coefficient decreases monotonically with the sweep. However, after $\chi = 60$ deg, the drag reduction due to the sweep becomes

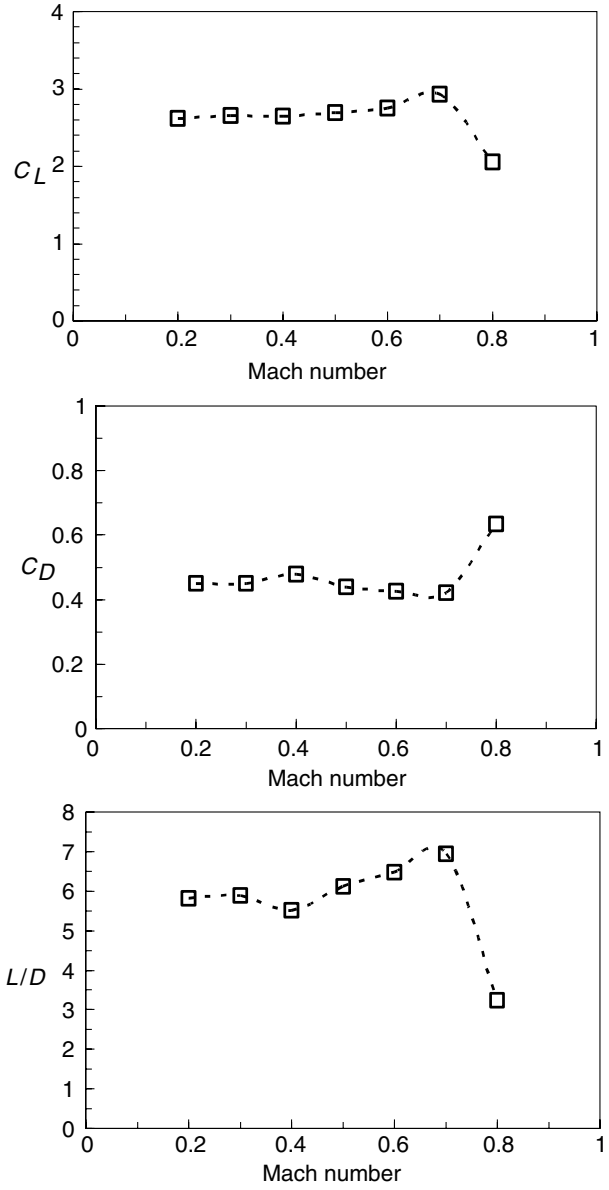

Fig. 2 Aerodynamic performances of the projectile with fully deployed wing at $\alpha = 0$ deg.

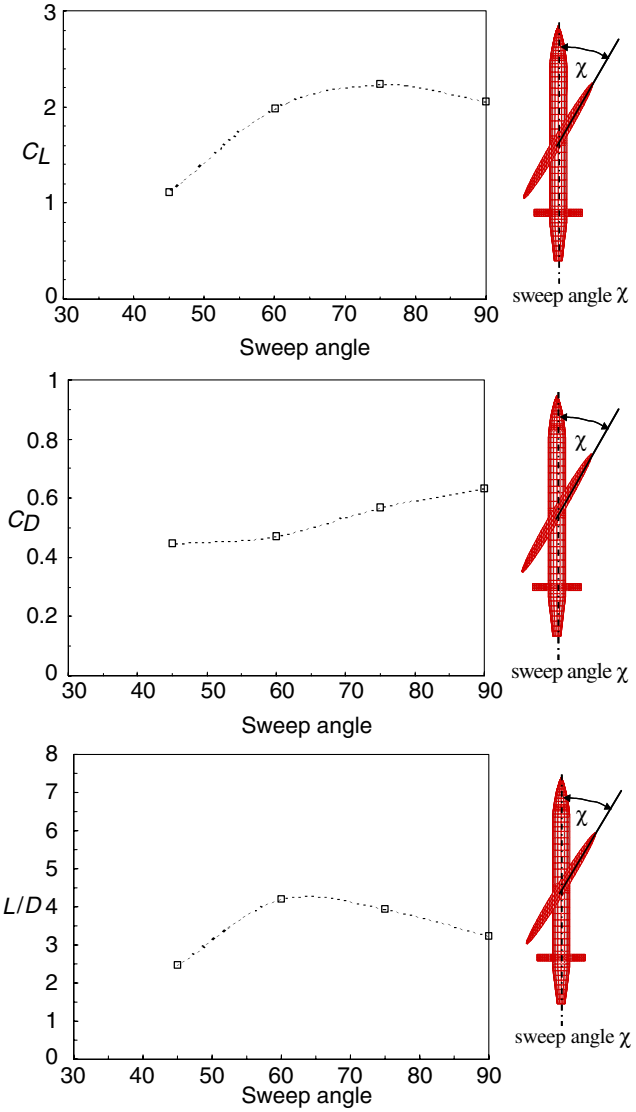

Fig. 4 Effects of sweep angles on aerodynamic performances of the projectile at $M_\infty = 0.8$.

significantly smaller. This indicates that from $\chi = 60$ deg, the transonic effects are no longer important. Further sweep of the wing will mainly reduce the lifting area but has a much smaller impact on the wave drag. Therefore, the lift-to-drag ratio of the projectile initially increases with the sweep and then decreases. It achieves the maximum value around $\chi = 60$ deg.

Figure 5 shows the pressure contours around the wing at the midspan for three different sweep angles. It is found that the first 15 deg sweep does not weaken the shock too much. The pressure contour plot at $\chi = 75$ deg is very close to the one at $\chi = 90$ deg. However, after another 15 deg sweep, the shock on the upper surface becomes pretty weak at $\chi = 60$ deg. And so, there is no need for further sweep, which can only effectively reduce the lifting area. The observations here support the results presented in Fig. 4.

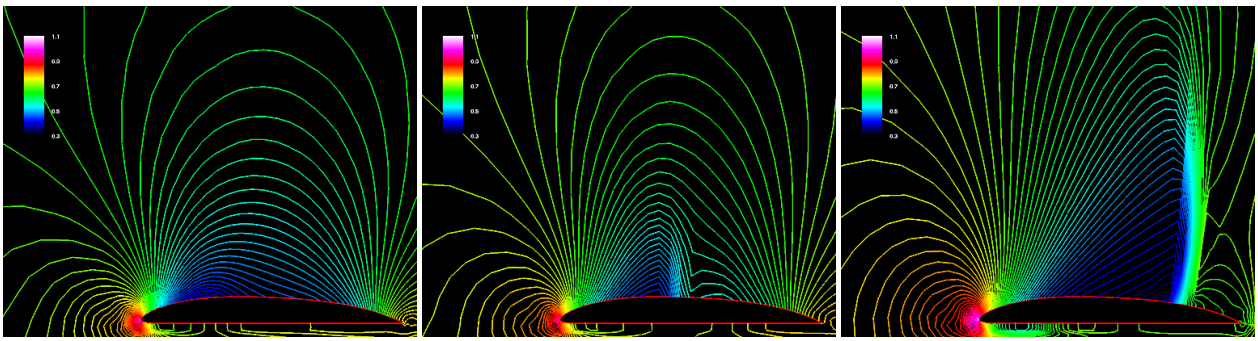

a) M_∞=0.6 **b) M_∞=0.7** **c) M_∞=0.8**

Fig. 3 Pressure contours around the wing at midspan for fully deployed cases.

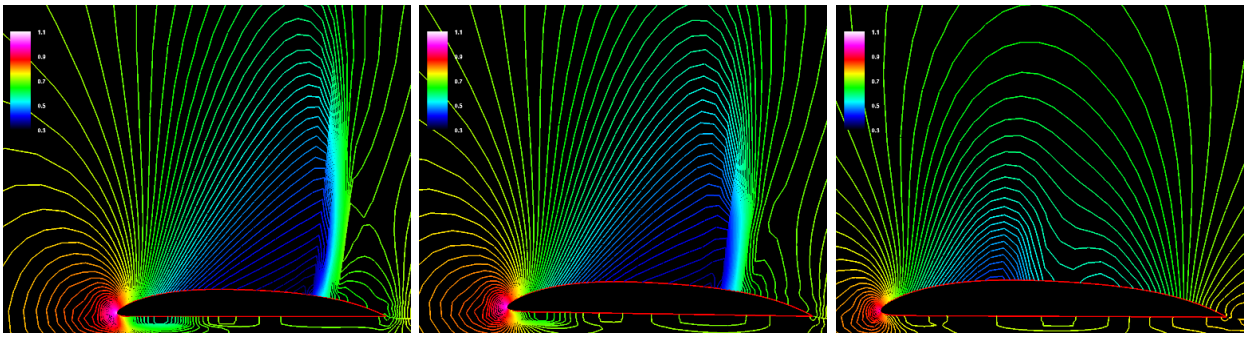

a) χ=90 deg b) χ=75 deg c) χ=60 deg

Fig. 5 Pressure contours around wing at midspan at $M_\infty = 0.8$.

C. Optimal Scheduling of the Wing at $\alpha = 0$ deg

Table 1 presents the lift-to-drag ratio of the projectile for both fully deployed and oblique-wing cases. Also given in the table are the sweep angles at which the maximum lift-to-drag ratio is achieved at several Mach numbers in the latter oblique-wing case. It is found that above the Mach number of 0.7, using oblique-wing strategy can significantly enhance the lift-to-drag ratio of the projectile.

Based on the preceding aerodynamic data, a simple two degrees-of-freedom trajectory analysis is further performed to investigate the effect of the oblique wing on the projectile range. Figure 6 shows the trajectory of the projectile with the exit Mach number of three and the elevation angle of 30 deg. It is found that using the oblique wing in the supersonic and transonic gliding phases can enhance the projectile range by more than 25%. Also shown in Fig. 6 is the history of Mach numbers of the projectile during the whole flight. It is found that in this case, during about 15% of the trajectory, the projectile needs to fly with the oblique wing to achieve higher L/D.

D. Effect of Angle of Attack

The preceding results are for $\alpha = 0$ deg case, in which the lift-to-drag ratio of the projectile is relatively low for all Mach numbers. In the following, we will explore the possibility of using higher angle of attack (AOA) to enhance the lift-to-drag ratio and therefore the projectile range.

For the $\alpha = 0$ deg case, we already know that the transonic effects are negligible up to $M_\infty = 0.7$. However, increasing α will lead the transonic effects to occur earlier. Figure 7 presents the lift-to-drag ratio of the projectile vs α for $M_\infty = 0.6$ and 0.7. It is found that for $\alpha < 2$ deg, the lift-to-drag ratio of the projectile at $M_\infty = 0.7$ is slightly higher than its counterpart at $M_\infty = 0.6$, but starts to drop below its counterpart at $M_\infty = 0.6$ for $\alpha \geq 2$ deg due to the stronger transonic effects. With increment of M_∞ from 0.6 to 0.7, the angle of attack corresponding to the maximum lift-to-drag ratio reduces from 5 to 3 deg, while the maximum lift-to-drag ratio decreases from 11.766 to 9.864. Nevertheless, compared with the corresponding lift-to-drag ratio at $\alpha = 0$ deg, these maximum lift-to-drag ratios for nonzero α are significantly improved. From the lift and drag curves shown in Fig. 7, it can also be seen that the transonic effects are mainly reflected in the rapid increment of the drag (wave drag) coefficient with α.

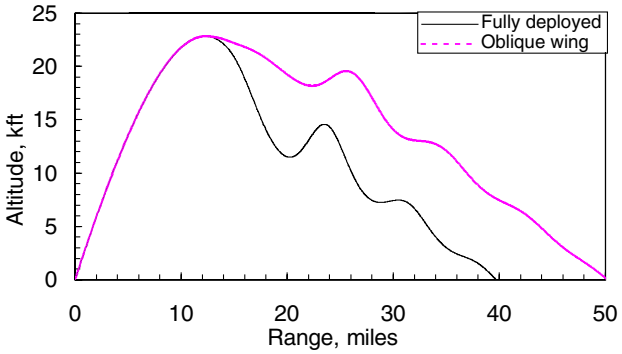

a) Trajectory

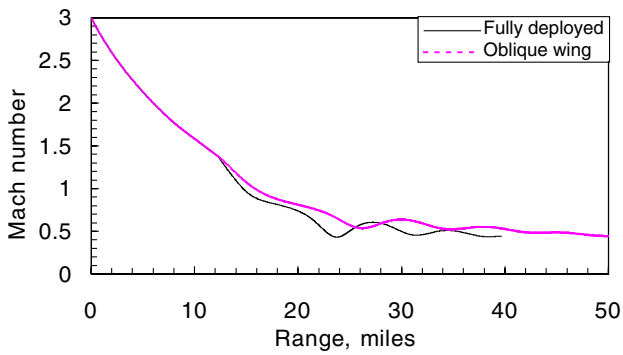

b) Mach number history

Fig. 6 Trajectory and Mach number distribution of the projectile with $M_{\text{exit}} = 3$ and $\theta = 30$ deg.

Table 1 L/D of the projectile for fully deployed and oblique-wing configurations at $\alpha = 0$ deg

M_∞	$(L/D)_{\chi=90\,\text{deg}}$	$(L/D)_{\max}$	χ
0.2	5.816	5.816	90 deg
0.3	5.889	5.889	90 deg
0.5	6.125	6.125	90 deg
0.6	6.481	6.481	90 deg
0.7	6.948	6.948	90 deg
0.8	3.238	4.197	60 deg
0.95	0.190	1.879	45 deg
1.05	0.132	1.527	45 deg
1.2	0.093	0.806	45 deg

E. Optimal Scheduling of the Wing for Maximum L/D

Up to this point, the optimal scheduling of the wing for the maximum lift-to-drag ratio can be determined from the computational results. Table 2 presents the optimal sweep angles and angles of attack, and the maximum achievable lift-to-drag ratios for ten different Mach numbers, ranging from 0.3 to 1.4.

Based on the preceding aerodynamic data, we further perform a simple two degrees-of-freedom trajectory analysis for the projectile with the exit Mach number of three and the elevation angle of 55 deg. It is found in Fig. 8 that using the preceding optimal scheduling of the wing, the averaged lift-to-drag ratio during the whole gliding phase can achieve 8.5 and the projectile range can be significantly

Table 2 Optimal scheduling and maximum L/D

M_∞	α	$(L/D)_{\max}$	χ
0.3	5 deg	90 deg	9.704
0.5	5 deg	90 deg	10.319
0.6	5 deg	90 deg	11.766
0.7	5 deg	60 deg	10.360
0.8	5 deg	45 deg	6.978
0.9	5 deg	45 deg	5.037
0.95	6 deg	45 deg	4.749
1.05	6 deg	45 deg	3.696
1.2	6 deg	45 deg	3.393
1.4	6 deg	30 deg	3.373

enhanced to more than 123 miles, which is about 107 n miles. This exceeds our target of 100 n miles. Also included in Fig. 8 is the variation of Mach numbers during the whole flight. For about 19% of the trajectory, the projectile needs to fly with the oblique wing to achieve higher L/D.

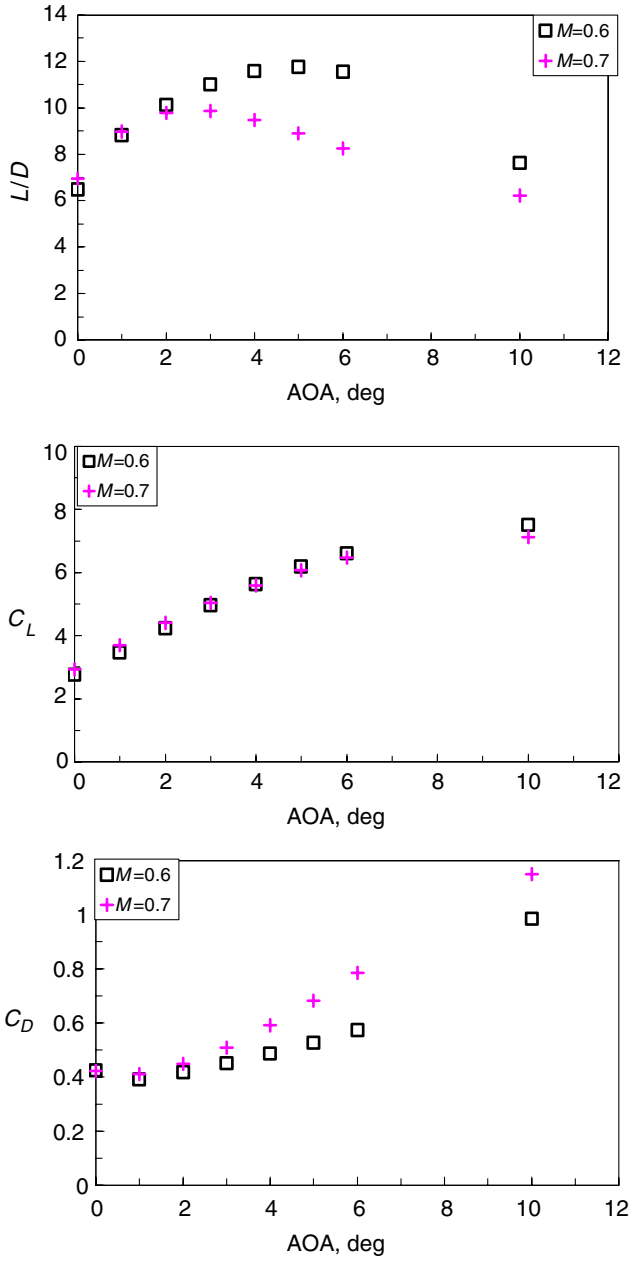

Fig. 7 Variation of aerodynamic forces with AOA.

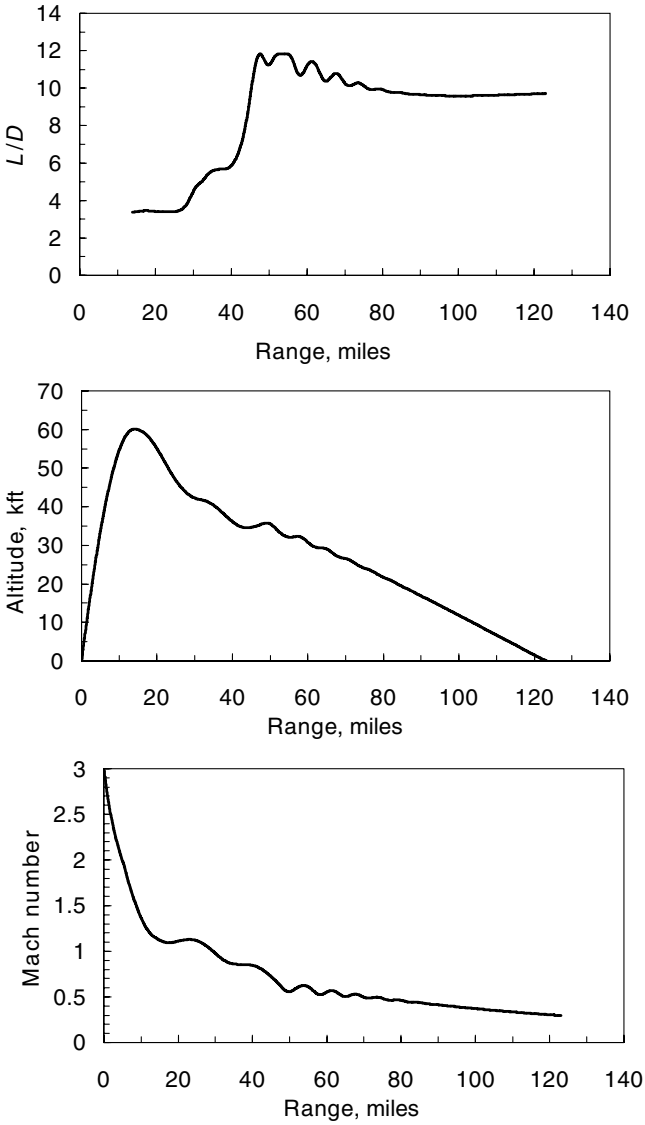

Fig. 8 L/D, trajectory, and Mach number distributions of the projectile with $M_{\text{exit}} = 3$ and $\theta = 55$ deg.

IV. Conclusions

Intensive thin-layer Reynolds-averaged Navier–Stokes computations are performed to determine the optimal scheduling of the oblique wing for a projectile during the supersonic and transonic gliding phases. It is found that by using the oblique-wing technique, a guided projectile can achieve the maximum lift-to-drag ratio throughout its gliding phase and therefore extend its range beyond the target 100 n miles without rocket assistance.

Acknowledgments

This work is sponsored by Navy Small Business Innovation Research (SBIR) phase 2 contract N00178-00-C-1051. The technical monitors are John Fraysse and David L. Liese. The first author also gratefully acknowledges R. T. Biedron of NASA Langley Research Center for his assistance in using PEGASUS overset data files in CFL3D and S. E. Rogers of NASA Ames Research Center for his help on setting up PEGASUS.

References

[1] Jones, R. T., *Wing Theory*, Princeton Univ. Press, Princeton, NJ, 1990.
[2] Macknight, N., *Tomahawk Cruise Missile*, Motorbooks International, Osceola, WI, 1995.

[3] Krist, S. L., Biedron, R. T., and Rumsey, C. L., CFL3D User's Manual Ver. 5.0, NASA Langley Research Center, Hampton, VA, 1998.
[4] Roe, P. L., "Approximate Riemann Solvers, Parameter Vectors, and Difference Schemes," *Journal of Computational Physics*, Vol. 43, Oct. 1981, pp. 357–372.
[5] Spalart, P., and Allmaras, S., "One-Equation Turbulence Model for Aerodynamic Flows," AIAA Paper 92-0439, Jan. 1992.
[6] Chan, W. M., Chiu, I.-T., and Buning, P. G., "User's Manual for the HYPGEN Hyperbolic Grid Generator and the HGUI Graphical User Interface," NASA TM-108791, Oct. 1993.
[7] Baysal, O., Fouladi, K., and Lessard, V. R., "Multigrid and Upwind Viscous Flow Solver on Three-Dimensional Overlapped and Embedded Grids," *AIAA Journal*, Vol. 29, No. 6, 1991, pp. 903–910.
[8] Suhs, N. E., Rogers, S. E., and Dietz, W. E., "PEGASUS 5: An Automated Pre-Processor for Overset-Grid CFD," AIAA Paper 2002-3186, June 2002.